Out-of-plane electron currents in magnetic islands formed during collisionless magnetic reconnection

Can Huang,[1] Quanming Lu,[1] Mingyu Wu,[1] San Lu,[1] and Shui Wang[1]

Received 17 July 2012; revised 28 December 2012; accepted 9 February 2013; published 28 March 2013.

[1] Secondary islands are considered to play a crucial role in collisionless magnetic reconnection. Based on 2-D particle-in-cell simulations, we investigate the characteristics of the out-of-plane electron currents in magnetic islands formed during collisionless magnetic reconnection with an initial guide field. In a primary island (formed simultaneously with the appearance of the X lines), due to the acceleration of the trapped electrons, the direction of the formed out-of-plane electron current is reverse to the original one. In the secondary island (formed in the vicinity of the X-line), the out-of-plane electron current is generated due to the accelerated electrons by the reconnection electric field in the vicinity of the X line. In such a way, the direction of the out-of-plane electron current in a secondary island is found to be opposite to that in a primary island. Such characteristics are found to be related to the evolution of the magnetic islands and then electron dynamics in the islands, which are proposed in this paper to be a possible criterion to identify a secondary island formed during collisionless magnetic reconnection, especially in the magnetotail.

Citation: Huang, C., Q. Lu, M. Wu, S. Lu, and S. Wang (2013), Out-of-plane electron currents in magnetic islands formed during collisionless magnetic reconnection, *J. Geophys. Res. Space Physics*, *118*, 991–996, doi:10.1002/jgra.50185.

1. Introduction

[2] As a fundamental physical process in plasma, magnetic reconnection is often invoked to explain the rapid conversion of magnetic energy into plasma kinetic and thermal energies [*Vasyliunas*, 1975; *Biskamp*, 2000; *Priest and Forbes*, 2000]. Therefore, magnetic reconnection is believed to be the major driving mechanism for many explosive phenomena in solar atmosphere [*Giovanelli*, 1946; *Masuda et al*., 1994], the Earth's magnetosphere [*Baker et al*., 1996; *Nagai et al*., 1998; *Angelopoulos et al*., 2008], laboratory experiments [*Ji et al*., 1998; *Li et al*., 2007; *Dong et al*., 2012], and even the magnetotail of a nonmagnetized planet [*Eastwood et al*., 2008; *Zhang et al*., 2012]. The characteristics of the ion diffusion region are considered to be the key point to understand the fast rate of collisionless magnetic reconnection, which is determined by the Hall effects caused due to ion-electron decoupling [*Sonnerup*, 1979; *Terasawa*, 1983; *Birn et al*., 2001; *Shay et al*., 2001; *Fu et al*., 2006; *Lu et al*., 2010].

[3] Recently, numerical studies have shown that the diffusion region is unstable and secondary magnetic islands may be formed in the vicinity of the X line. An extended electron current sheet is found to be formed in the vicinity of the X line in 2-D particle-in-cell (PIC) simulations of antiparallel magnetic reconnection with open boundary condition, where a secondary island may be produced and then ejected out [*Daughton et al*., 2006]. A new secondary island may be generated again and ejected out again, and such a process occurs periodically. *Daughton et al*. [2009] further found that secondary islands may also be generated in Sweet-Parker reconnection layers when the Lundquist number is sufficiently large. The extension of the electron current sheet and the formation of secondary islands have also been found in guide field reconnection, although now the current sheet becomes tilted because the accelerated electrons in the vicinity of the X line stream outward along only two of the four separatrices [*Drake et al*., 2005, 2006; *Daughton et al*., 2011]. The resulting secondary islands not only may affect the reconnection rate in both antiparallel and guide field reconnection [*Drake et al*., 2006; *Daughton et al*., 2006; *Huang et al*., 2011], but also can enhance the electron acceleration efficiency greatly in magnetic reconnection [*Wang et al*., 2010; *Oka et al*., 2010]. Therefore, it is crucial for us to know the characteristics of secondary islands. In this paper, based on 2-D PIC simulation results, we investigate the formation of out-of-plane electron currents in magnetic islands, and propose that the direction of the out-of-plane electron currents may provide a possible observation criterion to identify a secondary island in collisionless magnetic reconnection.

2. Simulation Model

[4] Two-dimensional PIC simulations are employed in this paper. In the PIC simulations, ions and electrons are treated as individual particles, and their trajectories are followed by integrating the Newton equation. The electromagnetic fields are defined in the grids, and can be known by solving the Maxwell equations with a full explicit algorithm. The details of the PIC simulation model can be

[1]CAS Key Laboratory of Geospace Environment, Department of Geophysics and Planetary Sciences, University of Science and Technology of China, Hefei 230026, China.

Corresponding author: Q. Lu, CAS Key Laboratory of Geospace Environment, Department of Geophysics and Planetary Sciences, University of Science and Technology of China, Hefei 230026, China. (qmlu@ustc.edu.cn)

2169-9380/13/10.1002/jgra.50185

referred in *Birdsall and Langdon* [1985]. Periodic boundary conditions are assumed in the x direction, and the particles leaving one boundary will reenter the other boundary. The ideal conducting boundary conditions for electromagnetic fields are employed in the z direction. The 1-D Harris current sheet is used as the initial configuration in the present simulations [*Harris*, 1962], and profile of the magnetic field is

$$\mathbf{B}_0(z) = B_0 \tanh(z/\delta)\mathbf{e}_x + B_{y0}\mathbf{e}_y, \quad (1)$$

where B_0 and δ are the asymptotical magnetic field and the initial half-width of the current sheet, respectively. Here B_{y0} is the amplitude of the initial guide field, which is set to be $B_{y0} = -B_0$ in our simulations. The corresponding profile of the number density is

$$n(z) = n_b + n_0 \,\mathrm{sech}^2(z/\delta), \quad (2)$$

where n_b represents the density of the uniform, background plasma while n_0 is the peak Harris density. The distributions of ions and electrons are assumed to satisfy the Maxwellian function. The background plasma is nondrifting, while the drift speeds in the y direction of the Harris plasma satisfy $V_{i0}/T_{i0} = -V_{e0}/T_{e0}$ (where T_{i0} and T_{e0} are the initial ion and electron temperatures, while V_{i0} and V_{e0} are the initial ion and electron drift speeds). In our simulations, the initial density ratio is set to be $n_0 = 5n_b$. We choose $\delta = 0.5c/\omega_{pi}$ (where c/ω_{pi} is the ion inertial length based on the peak Harris density n_0). The mass ratio is set to be $m_i/m_e = 100$ (where m_i is the mass of the ion, and m_e is the rest mass of the electron), and the light speed is $c = 15v_A$, where v_A is the Alfvén speed based on B_0 and n_0. Two simulation cases (Runs 1 and 2) are performed in this paper. The initial temperature ratio is set to be $T_{i0}/T_{e0} = 4$ and 0.5 in Runs 1 and 2, respectively.

[5] The computation is carried out in a rectangular domain in the (x,z) plane. The simulation box employed in this paper has a size of $L_x = 51.2c/\omega_{pi}$ in the x direction and a size $L_z = 12.8c/\omega_{pi}$ in the z direction with $N_x \times N_z = 1024 \times 256$ grids, so the spatial resolution is $\Delta x = \Delta z = 0.05c/\omega_{pi} = 0.5c/\omega_{pe}$ (where c/ω_{pe} is the electron inertial length based on the peak Harris density n_0). The time step is set to $\Omega_i \Delta t = 0.001$, where $\Omega_i = eB_0/m_i$ is the ion gyrofrequency. More than 300 particles per cell, on average, are employed in the simulations. An initial flux perturbation is introduced to make the system reach the stage of a rapid growth of the reconnection rate quickly.

3. Simulation Results

[6] In Run 1, $T_{i0}/T_{e0} = 4$, and the initial current in the Harris current sheet is mainly carried by ions. Figure 1 shows the contour of the out-of-plane electron current J_{ey} at $\Omega_i t = 0$, 10, 20, 27, and 32 for Run 1. The magnetic field lines are also plotted in the figure for reference. Initially, the electron current is positive, and it is along the y direction. This is a multiple X line reconnection. With the proceeding of the reconnection, two X lines are formed at about $x = 0$ and $x = 26c/\omega_{pi}$, and two magnetic islands are formed between them. Here we define a magnetic island, which is formed simultaneously with the appearance of the X lines, as a primary island. The width of the primary island will increase in the z direction, and it is about $6c/\omega_{pi}$ at the saturation stage. At the same time, the electrons in the vicinity of the X lines are accelerated along the $-y$ direction by the reconnection electric field. Then an

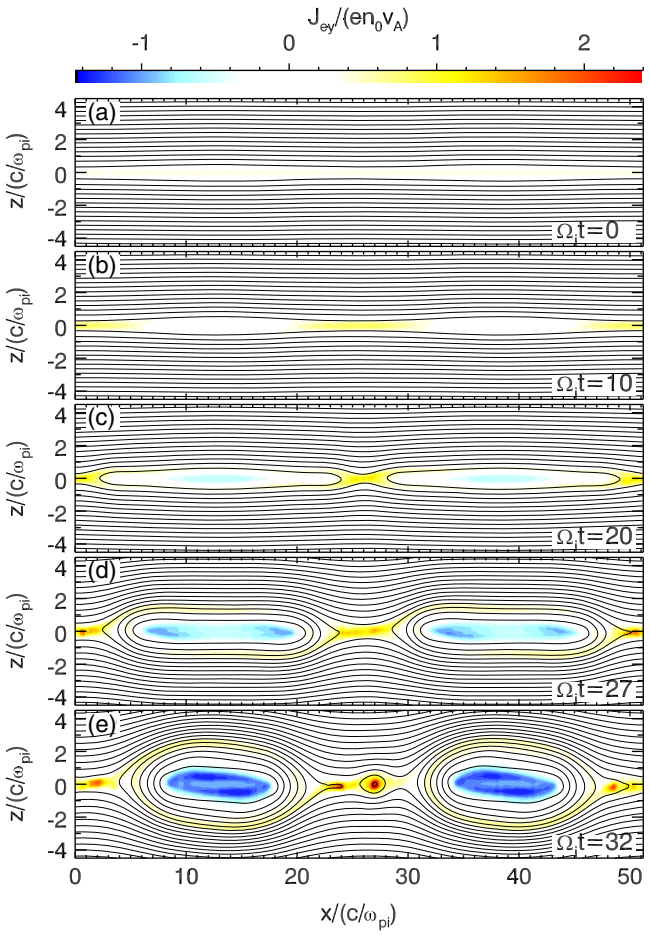

Figure 1. The time evolution of the out-of-plane electron current density J_{ey} at $\Omega_i t = 0$, 10, 20, 27, and 32 for Run 1. The solid lines represent the in-plane magnetic field lines.

electron current sheet, where the current is carried mainly by the electrons, is formed. We can find that the electron current sheet in the vicinity of the X line, which is around $x = 26c/\omega_{pi}$, is extended in the x direction. It is unstable to the tearing instability and a secondary island is then formed [*Huang et al.*, 2011]. Here an island, which is formed in the vicinity of the X line, is called as a secondary island. Obviously, the out-of-plane electron current in the primary islands is negative, and the electron flow is along the $+y$ direction. In the secondary island, the out-of-plane electron current is positive, and the electron flow is along the $-y$ direction.

[7] The characteristics of the out-of-plane electron currents in the primary and secondary islands can be demonstrated more clearly in Figure 2, which shows the profiles of the total current (solid lines), ion current (dashed lines) and electron current (dotted lines) in (a) the secondary island and (b) the primary island at $\Omega_i t = 27$ for Run 1. The profiles of the currents in the secondary and primary islands are obtained along the lines $x = 27c/\omega_{pi}$ and $x = 39c/\omega_{pi}$, respectively. Obviously, in the secondary island, the out-of-plane current, which is mainly carried by electrons, is positive with the peak about $3.0en_0v_A$, while the contribution of ions is almost negligible. In the primary island, the contributions of ions and electrons to the out-of-plane currents are comparable, and the out-of-plane electron current is negative with the

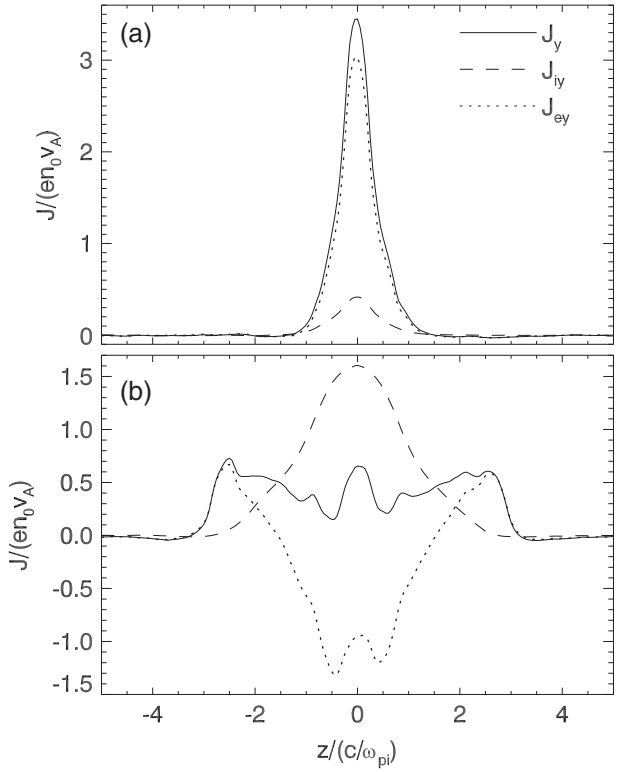

Figure 2. The profiles of the total current (solid lines), ion current (dashed lines), and electron current (dotted lines) in (a) the secondary island and (b) the primary island at $\Omega_i t = 27$ for Run 1.

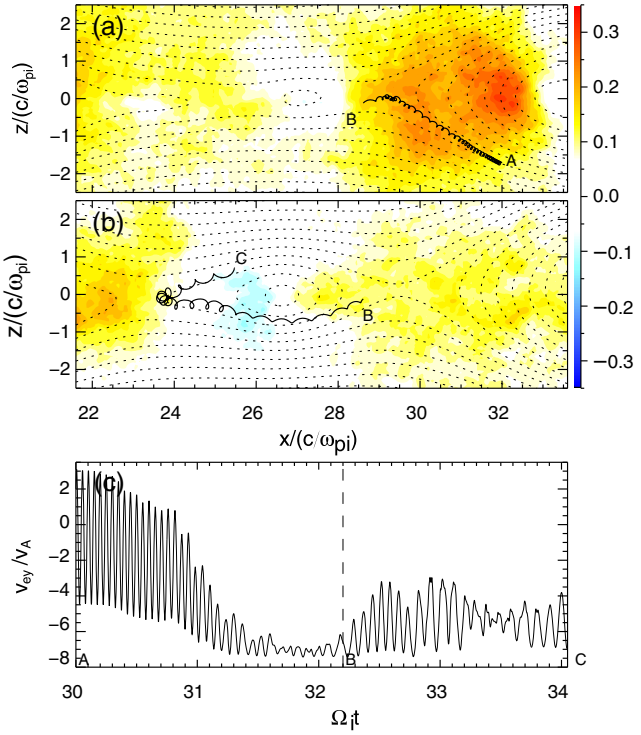

Figure 3. A typical electron trajectory in the (x, z) plane during (a)$30 \le \Omega_i t \le 32.2$, (b)$32.2 \le \Omega_i t \le 34$, and the evolution of the velocity in the y direction v_{ey} for Run 1. The magnetic field lines (dotted contours) and the reconnection electric field E_y (filled contours) at $\Omega_i t =$ (a) 30 and (b) 33.5 are also plotted in the figure for reference.

peak about $1.3en_0v_A$. We can also find that the at the edge of the primary island, the out-of-plane current is positive.

[8] In the vicinity of the X line, the electrons are accelerated along the $-y$ direction by the reconnection electric field. Therefore, it is easy to understand that the out-of-plane electron current in a secondary island is positive, because a secondary island is formed in the extended electron current sheet. Figure 3 shows a typical electron trajectory in the (x, z) plane and the evolution of the velocity in the y direction from $\Omega_i t = 30$ to $\Omega_i t = 34$ for Run 1; the electron is at last trapped in the secondary island. The magnetic field lines and the reconnection electric field E_y are also plotted in the figure for reference. The electron is accelerated in the $-y$ direction by the reconnection electric field when it enters the vicinity of the X line. At the same time, the secondary island is formed in the vicinity of the X line, and the electron is trapped by the secondary island. The trapped electron has a large velocity in the $-y$ direction. In this way, the formed out-of-plane electron current in the secondary island has a positive value.

[9] The formation of the out-of-plane electron current in a primary island can also be understood by following the electron trajectories. Figure 4 shows a typical electron trajectory in the primary island for Run 1. Figures 4a and 4b exhibit the electron trajectory in the (x, z) plane and the evolution of the gyrocenter velocity in the y direction (v_{Gy}), respectively. In the calculation, a fixed electromagnetic field, which is obtained from the simulations at $\Omega_i t = 27$, is used. The magnetic field lines are also plotted in the figure for reference. Initially, the electron is located at A. The electron can be obviously accelerated in the y direction at the two ends of the island, which is during the

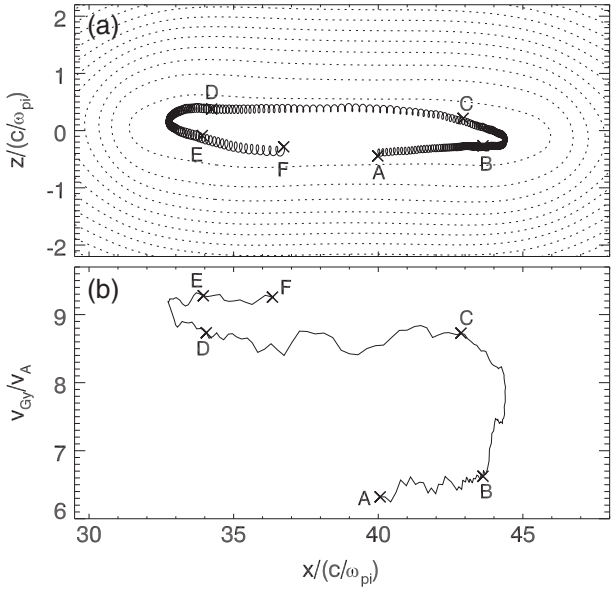

Figure 4. (a) A typical electron trajectory in the (x, z) plane in the primary island, and (b) the evolution of electron gyrocenter velocity in the y direction (v_{Gy}) for Run 1. The start and end points are denoted by A and F, respectively. In the calculation, a fixed electromagnetic field, which is obtained from the simulations at $\Omega_i t = 27$, is used. The start and end points are denoted by A and F, respectively.

period from B to C and D to E. During the period from B to C, the velocity of the electron gyrocenter in the y direction is accelerated from about $6.5v_A$ to about $8.7v_A$. Then, the electron drifts along the $-x$ direction during the period from C to D. During the period from D to E, the velocity of the electron gyrocenter in the y direction gets further accelerated to about $9.3v_A$. Therefore, the electrons in the primary island are accelerated in the $+y$ direction, which leads to a negative electron current in the island. The particle is accelerated at the two ends of the primary island due to the existence of the electric field in these regions. According to a two-fluid model for the plasma, the electric field can be expressed as $\mathbf{E} = -\mathbf{V}_e \times \mathbf{B} - \frac{\nabla \cdot \vec{\mathbf{P}}_e}{en_e} - \frac{m_e}{e}\frac{d\mathbf{V}_e}{dt}$. In general, the electron inertial term $-\frac{m_e}{e}\frac{d\mathbf{V}_e}{dt}$ is negligible. While in these regions, the electric field is determined mainly by the electromotive force term $-\mathbf{V}_e \times \mathbf{B}$, which is demonstrated in Figure 5. Figure 5 plots the profiles of the electric field (a) E_y and (b) E_z along $z=0$ in the primary island at $\Omega_i t=27$ for Run 1. The electric field E_x is much smaller than E_y and E_z, and we do not plot it in the figure. Obviously, in the primary island, the electric field is determined mainly by the electromotive force term, which is due to the compression of the island. One thing that should be noted is that only the electrons, whose initial energy is sufficiently large, can be nonadiabatically accelerated in the island when their gyroradii are comparable to the curvature radii of the magnetic field lines. Such a mechanism of the electron acceleration in a magnetic island has already been studied by *Fu et al.* [2006] and *Drake et al.* [2006]. These accelerated electrons form the out-of-plane electron current in the primary island.

[10] To verify our conclusions about the out-of-plane electron current in magnetic islands, an additional case is performed. In this case (Run 2), the initial temperature ratio

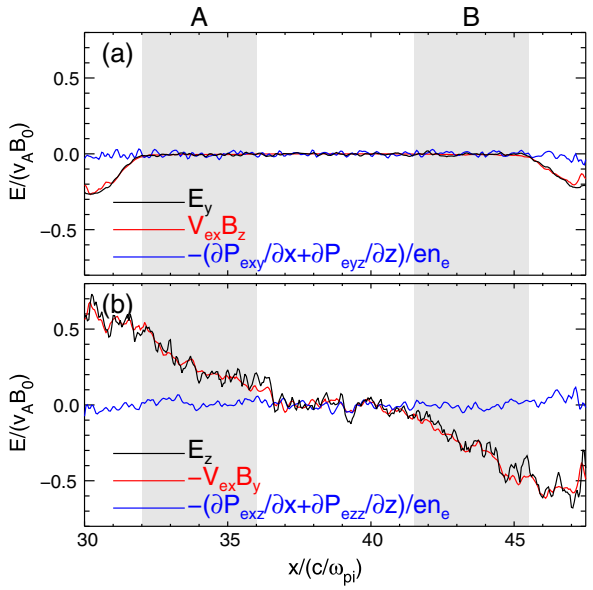

Figure 5. The profiles of the electric field (a) E_y and (b) E_z and along $z=0$ in the primary island at $\Omega_i t=27$ for Run 1. The electron motion term (red curves) and pressure tensor term (blue curves) and also plotted. Electrons are mainly accelerated in the y direction in Regions A and B, which are denoted by gray areas.

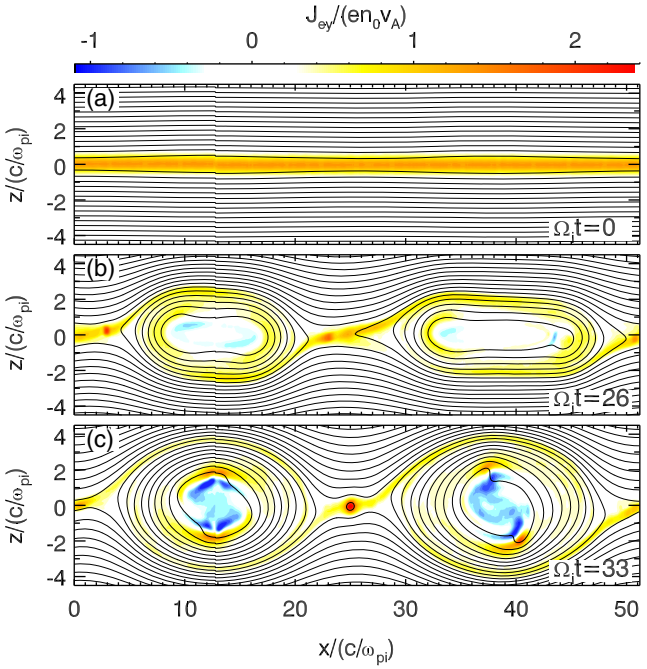

Figure 6. The time evolution of the out-of-plane electron current density J_{ey} at $\Omega_i t=0$, 26, and 33 for Run 2. The solid lines represent the in-plane magnetic field lines.

T_i/T_e is set to be 0.5, and the initial current in the Harris current sheet is mainly carried by electrons. Figure 6 shows the contours of the out-of-plane electron current J_{ey} at $\Omega_i t=0$, 26, and 33 for Run 2. Initially, the out-of-plane electron current is positive. With the proceeding of the reconnection, two X lines are formed and two magnetic islands are formed between them. At $\Omega_i t=26$, an electron current sheet in the center of the simulation domain is formed. At $\Omega_i t=33$, a secondary island is born. Obviously, the out-of-plane electron current in the primary islands is negative, while the out-of-plane electron current in the secondary island is positive.

[11] We also plot the profiles of the out-of-plane currents inside the secondary and primary islands. Figure 7 shows the profiles of out-of-plane currents obtained along $x=25c/\omega_{pi}$ and $x=38.5c/\omega_{pi}$ at $\Omega_i t=33$. The out-of-plane current inside the secondary island is mainly carried by electrons, while the electron current is positive with a peak value around $2.6en_0v_A$. However, in the center of the primary island, the out-of-plane current is carried by both ions and electrons, while the out-of-plane electron current is negative. At the edge of the primary island, the out-of-plane electron current is positive. The formation mechanism of the out-of-plane electron current is the same as that in Run 1.

4. Conclusions and Discussion

[12] Secondary islands are considered to be able to affect the reconnection rate [*Daughton et al.*, 2006; *Huang et al.*, 2011], and they can also enhance the electron acceleration efficiency greatly [*Wang et al.*, 2010; *Oka et al.*, 2010]. However, the role of secondary islands in collisionless magnetic reconnection remains a central and unresolved issue. In this paper, by performing 2-D PIC simulations, we found that the direction of the out-of-plane electron current in the

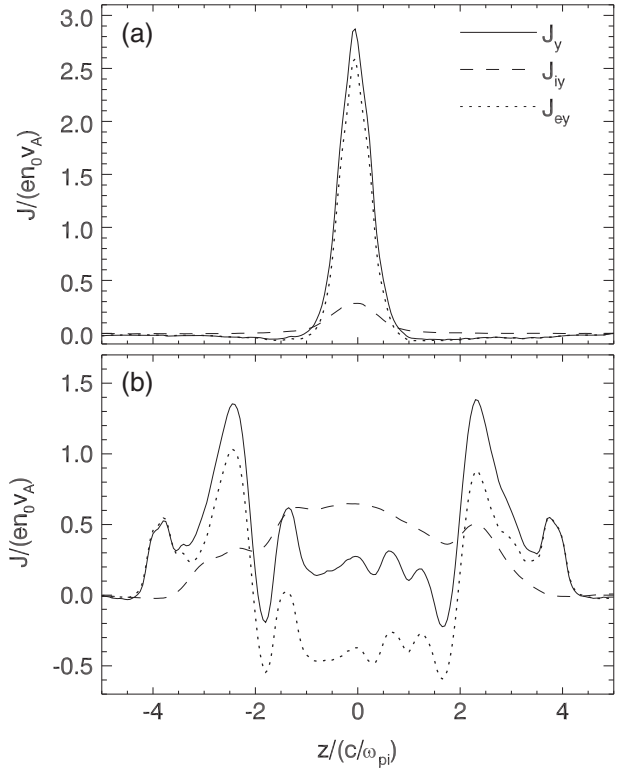

Figure 7. The profiles of the total current (solid lines), ion current (dashed lines), and electron current (dotted lines) in (a) the secondary island and (b) the primary island at $\Omega_i t = 33$ for Run 2.

secondary island is opposite to that in the primary island, although both the secondary island and primary island have the bipolar structure in B_z. The opposite out-of-plane electron currents have also been found by *Drake et al*. [2006] (see Figures 1 and 2). We further find that the out-of-plane electron current in the secondary island is formed due to electron acceleration by the reconnection electric field in the vicinity of the X line. The out-of-plane electron current in the primary island is related to the acceleration of the trapped electrons by the island, and the acceleration is due to the compression of the island. Such a mechanism of electron acceleration in magnetic island has already been studied by *Fu et al*. [2006] and *Drake et al*. [2006]. At the same time, these electrons obtain a large velocity in the $+y$ direction, and the out-of-plane electron current in the $-y$ direction is generated in the primary island. We also find that in the center of the primary island the region with the formed negative out-of-plane electron current become smaller with the decrease of T_{i0}/T_{e0} (also the initial the ion current). The characteristics of the out-of-plane electron currents in the secondary and primary islands may provide a possible observation criterion to identify a secondary island during collisionless magnetic reconnection, especially in the magnetotail, where the ion temperature is usually larger than the electron temperature.

[13] **Acknowledgments.** This research was supported by the National Science Foundation of China, grant 41204103, 11220101002, 41274144, 41174124, 40931053, 41121003, the 973 Program (2012CB825602), CAS Key Research Program KZZD-EW-01, Ph.D. Programs Foundation of Ministry of Education of China (20123402120010), Ocean Public Welfare Scientific Research Project, State Oceanic Administration People's Republic of China (201005017), open research fund from SOA Key Laboratory for Polar Science (KP201205), and the Fundamental Research Funds for the Central Universities (WK2080000010).

References

Angelopoulos, V., et al. (2008), *Science*, *324*, 1391-c.

Baker, D. N., T. I. Pulkkinen, V. Angelopoulos, W. Baumjohann, and R. L. McPherron (1996), Neutral line model of substorms: Past results and present view, *J. Geophys. Res.*, *101*, 12975-13010.

Birdsall, C. K., and A. B. Langdon (1985), *Plasma Physics via Computer Simulation*, pp. 351–359, Mcgraw-Hill Book Company, New York.

Birn, J., et al. (2001), Geospace Environmental Modeling (GEM) Magnetic Reconnection Challenge, *J. Geophys. Res.*, *106*, 3715, doi:10.1029/1999JA900449.

Biskamp, D. (2000), *Magnetic Reconnection in Plasmas*, p. 3, Cambridge Univ. Press, Cambridge, U. K.

Daughton, W., J. Scudder, and H. Karimabadi (2006), Fully kinetic simulations of undriven magnetic reconnection with open boundry conditions, *Phys. Plasmas*, *13*, 072101, doi:10.1063/1.2218817.

Daughton, W., V. Roytershteyn, B. J. Albright, H. Karimabadi, L. Yin, and K. J. Bowers (2009), Transition from collisional to kinetic regimes in large-scale reconnection layers, *Phys. Res. Lett.*, *103*, 065004, doi:10.1103/PhysRevLett.103.065004.

Daughton, W., V. Roytershteyn, H. Karimabadi, L. Yin, B. J. Albright, B. Bergen, and K. J. Bowers (2011), Role of electron physics in the development of turbulent magnetic reconnection in collisionless plasmas, *Nat. Phys.*, *7*, 539-542, doi:10.1038/nphys1965.

Dong, Q. L., et al. (2012), Plasmoid ejection and secondary current sheet generation from magnetic reconnection in laser-plasma interaction, *Phys. Rev. Lett.*, *215001*.

Drake, J. F., M. A. Shay, and W. Thongthai (2005), Production of Energetic Electrons during Magnetic Reconnection, *Phys. Rev. Lett.*, *94*, 095001, doi:10.1103/PhysRevLett.94.095001.

Drake, J. F., M. Swisdak, K. M. Schoeffler, B. N. Rogers, and S. Kobayashi (2006), Formation of secondary islands during magnetic reconnection, *Geophys. Res. Lett.*, *33*, L13105, doi:10.1029/2006GL025957.

Eastwood, J. P., D. A. Brain, J. S. Halekas, J. F. Drake, T. D. Phan, M. Oieroset, D. L. Mitchell,, R. P. Lin, and M. Acuna (2008), Evidence for collisionless magnetic reconnection at Mars, *Geophys. Res. Lett.*, *35*, L02106, doi:10.1029/2007GL032289.

Fu, X. R., Q. M. Lu, and S. Wang (2006), The process of electron acceleration during colisionless magnetic reconnection, *Phys. Plasmas*, *13*, 012309.

Giovanelli, R. G. (1946), A theory of chromospheric flares, *Nature*, *158*, 81, doi:10.1038/158081a0.

Harris, E. G. (1962), On a plasma sheath separating regions of oppositely directed magnetic field, *Nuovo Cimento Soc. Ital. Fis.*, *23*, 115, doi:10.1007/BF02733547.

Huang, C., Q. M. Lu, Z. W. Yang, M. Y. Wu, Q. L. Dong, and S. Wang (2011), The evolution of electron current sheet and formation of secondary islands in guide field reconnection, *Nonlinear Processes Geophys.*, *18*, 727-733, doi:10.5194/npg-18-727-2011.

Ji, H. T., M. Yamada, S. Hsu, and R. Kulsrud (1998), Experimental Test of the Sweet-Parker odel of magnetic reconnection, *Phys. Rev. Lett.*, *80*, 3256-3259.

Li, C. K., F. H. Seguin, J. A. Frenje, J. R. Rygg, R. D. Petrasso, R. P. J. Town, O. L. Landen, J. P. Knauer, and V. A. Smalyuk (2007), Observation of Megagauss-field topology changes due to magnetic reconnection in laser-produced plasmas, *Phys. Rev. Lett.*, *99*, 055001.

Lu, Q. M., C. Huang, J. L. Xie, R. S. Wang, M. Y. Wu, A. Vaivads, and S. Wang (2010), Features of separatrix regions in magnetic reconnection: Comparison of 2-D particle-in-cell simulations and Cluster observations, *J. Geophys. Res.*, *115*, A11208, doi:10.1029/2010JA015713.

Masuda, S., T. Kosugi, H. Hara, and Y. Ogawara (1994), A loop top hard X-ray in a compact solar-flare as evidence for magnetic reconnection, *Nature*, *371*, 495-497.

Nagai, T., M. Fujimoto, Y. Saito, S. Machida, T. Terasawa, R. Nakamura, T. Yamamoto, T. Mukai, A. Nishida, and S. Kokubun (1998), Structure and dynamics of magnetic reconnection for substorm onsets with Geotail observations, *J. Geophys. Res.*, *103*, 4419-4440.

Oka, M., M. Fujimoto, I. Shinohara, and T. D. Phan (2010), "Island surfing" mechanism of electron acceleration during magnetic reconnection, *J. Geophys. Res.*, *115*, A08223, doi:10.1029/2010JA015392.

Priest, E., and T. Forbes (2000), *Magnetic Reconnection: MHD Theory and Applications*, p. 6, Cambridge Univ. Press, Cambridge, U. K.

Shay, M. A., J. F. Drake, B. N. Rogers, and R. E. Denton (2001), Alfvénic collisionless magnetic reconnection and the Hall term, *J. Geophys. Res.*, *106*, 3759, doi:10.1029/1999JA001007.

Sonnerup, B. U. Ö. (1979), Magnetic field reconnection, in *Solar System Plasma Physics*, vol. *3*, edited by L. J. Lanzèerotti, C. F. Kennel, and E. N. Parker, 46 pp., North-Holland, New York.

Terasawa, T. (1983), Hall current effect on tearing mode instability, *Geophys. Res. Lett.*, *10*, 475-478, doi:10.1029/GL010i006p00475.

Vasyliunas, V. M. (1975), Theoretical models of magnetic field line merging, *Rev. Geophys. Space Phys.*, *13*, 303-336, doi:10.1029/RG013i001p00303.

Wang, R. S., Q. M. Lu, A. M. Du, and S. Wang (2010), In situ observations of a secondary magnetic island in ion diffusion region and associated energetic electrons, *Phys. Rev. Lett.*, *104*, 175003, doi:10.1103/PhysRevLett.104.175003.

Zhang T. L., et al. (2012), Magnetic reconnection in the near venusian magnetotail, *Science*, *336*, 567-570, doi:10.1126/science.1217013.